Graduate University of Advanced Technology

Journal of Geological Remote Sensing

Journal homepage: https:// jgrs.kgut.ac.ir

Iranian Geological Remote Sensing Society

Application of Multisensor images for exploration of porphyry copper mineralization in the Rabor area, Kerman, Iran

A.Pourshamsoddin Motlagh[1*], H. Ranjbar[2]

[1] *Phd student, Department of Mining Engineering, Shahid Bahonar University of Kerman, Islamic Republic of Iran*
[2] *Professor, Department of Mining Engineering, Shahid Bahonar University of Kerman, Islamic Republic of Iran*

Article Info

Keywords:
Multisensor images
Remote sensing
Hydrothermal alterations
Porphyry Copper Deposits
Rabor
Kerman Province

Abstract

The purpose of this study is to use the multisensor images for the exploration of porphyry copper deposits in the southwest of Kerman province, Rabor region. In order to conduct this study, ASTER, Sentinel-2A and IKONOS images were used. First, IARR correction was performed on IKONOS, Sentinel-2A and 5 bands of the ASTER TIR dataset and FLAASH correction was applied on ASTER VNIR-SWIR bands, respectively. Then, upon initial identification of alteration zones and geochemical anomalies, these hydrothermal alterations and anomalies were surveyed and 37 samples were collected for laboratory studies. Thin sections were prepared and studied under the microscope, and selected samples were used for spectroradiometric study. Argillic, sericitic and propylitic hydrothermal alteration zones were identified with Spectral Feature Fitting (SFF) method by using samples' spectra. Iron oxide minerals were also characterized using the b4/b2 ratio of Sentinel-2A and b3/b1 ratio of IKONOS. Bands 2 and 4 of Sentinel-2A were combined with ASTER SWIR data for identifying areas with sericitic and argillic alteration types that are stained with iron oxides. The results of the combination of the selected bands of Sentinel-2A and ASTER images gave better results due to the higher resolution. Field observations and laboratory studies were used to validate the results. Geochemical Mineral Potential Index (GMPI) method also identified porphyry copper potential areas and was used as a validation method. Finally, the alteration zones were subdivided into eight zones for detailed exploration.

* Corresponding author.
Email: pourshams@eng.uk.ac.ir
https://doi.org/10.48306/ jgrs.2023.376483.1001
Received 16 Dec. 2022; Received in revised form 9 May 2023; Accepted 9 July 2023
Available online August 2023

1. Introduction

In the hydrothermal alteration environments associated with porphyry copper deposits, there are various minerals such as muscovite, kaolinite, chlorite and calcite, each with its own spectral properties that can be used in the preliminary stage of mineral exploration. Surface weathering has led to the formation of minerals such as jarosite, hematite and goethite (Lowell and Gilbert, 1970; Atapour and Aftabi, 2007). The ASTER and Sentinel-2A data are capable of mapping these minerals (Van der Meer and Van der Wreff, 2016; Mars and Rowan, 2006).

Different methods of image processing of ASTER images for exploratory and geological studies are seen in various studies (Abrams et al., 1983; Gupta, 2003; Honarmand et al., 2013; Khaleghi et al., 2020; Mars and Rowan, 2006; Alimohammadi et al., 2015; Masoumi et al., 2017; Yousefi et al., 2018a, Honarmand et al., 2018). Landsat and Sentinel- 2A images are also used in many studies (Yousefi et al., 2018b; Jain et al., 2018; Yan et al., 2016; Voulo et al., 2016; Bahrami et al., 2021; Chen et al., 2022; Van der Meer and Van der Wreff, 2016).

The purpose of this research is to use different satellite images (ASTER, Sentinel-2A and IKONOS) to explore areas with porphyry copper potential in the southwest of Kerman province, Rabor district. As the porphyry copper deposits are associated with sericitic, argillic, and propylitic hydrothermal alteration types, the PCA (Principal Component Analysis) and the SFF (Spectral Feature Fitting) methods can be used for their identification.

PCA is a multivariate statistical method that is used to reduce the volume of data and also identify the minerals based on their spectral properties that manifest themselves as higher and lower loadings with opposite mathematical signs in selected PCs. The application of this method for processing satellite images has been seen in many studies (e. g. Crosta et al., 2003; Tangestani et al., 2005; Mars and Rowan, 2006; Shahriari et al., 2013). In order to extract more information from different sensor bands, it is best to consider the combination of bands from different sensors. Crosta et al. (2003) used PCA method for the mapping of different minerals. They have introduced the method of selecting the bands based on the spectrum of the desired mineral. By using this method, based on spectral properties of minerals, suitable bands are selected for mineral identification.

SFF is a mapping method based on the comparison of absorption features between the images and the standard spectrum (Abbaszadeh and Hezarkhani, 2013). The standard spectrum is obtained from ground or laboratory sample or can be extracted from the desired images.

Furthermore, Geochemical Mineralization Probability Index (GMPI) is used as a potential mineralization method that is consistent with the concept of probability and a method for weighting classes of geochemical anomalies. The basis of this method is the stepwise PCA selection using factor analysis (Yousefi et al., 2012). GMPI was first applied by Yousefi et al. (2012) on stream sediments geochemical data of two geological sheets (Baft and Sarduiyeh, southeastern Iran). In addition to field observations and laboratory studies, this method was used as an evidence data of different nature for verifying the hydrothermal alteration associated with mineralization.

2. Geology

The study area is located in the Urmia-Dokhtar volcanic belt, as a part of which is known as Dehaj-Sarduiyeh in Kerman province (Dimitrijević, 1973). Geological map of the region was prepared by a Geological group of the former Yugoslavia in 1972, on behalf of the Geological Survey of Iran at a scale of 1: 100,000. Geological information for this study was extracted from this map (Figure 1).

The highest elevation of the area is located in the Shah Kuh, northwest of the area with a height of 4376 meters. The Rabor and Roudbar are the main

rivers in the central part of the region. The study area has five geological units in summary: 1. Quaternary rocks that are commonly found in the southern portion; 2. Neogene volcanic rocks, which outcrop in the northwest of the area and a smaller part in the southern part of the area; 3. Miocene-Pliocene sediments, which comprise the major part of the sedimentary rocks of the southern part of the area; 4. Intrusive masses with Miocene age that are intruded the Eocene volcanic rocks, and 5. Eocene volcanic rocks that have the largest geological units in the region. These rocks are mostly found in the central parts of the area and are found mainly around intrusive masses. Miocene granitoid rocks are found in the central and northern parts of the area and are the main constituents of Shah Kuh (Mount of Lalehzar). These intrusive masses have been hydrothermally altered in some areas and are associated with Cu mineralization in some areas. The mineralization types in this area are mainly porphyry type (Pay Negin, Lalehzar 3 and 4) and vein type (lead and zinc of QanatMarvan), which are formed along various deposits located on Urmia-Dokhtar volcanic-sedimentary belt (Dimitrijević, 1973).

3. Materials and methods

Known Porphyry copper deposits are directly linked to the hydrothermal alterations pattern (potassic, phyllic, argillic, and propylitic) suggested by Lowell and Gilbert (1970) and the iron oxide cap that is formed above these deposits, as a result of surficial oxidation. The minerals formed in the processes of hydrothermal alteration and surficial oxidation, can be mapped using multisensor images such as ASTER, Landsat 9, and Sentinel-2A.

In each of the sericitic, argillic, silicic, propylitic, and also gossans in copper deposits, at least one of the existing alteration minerals has a unique spectral property in the VNIR, SWIR, and TIR ranges. Identification of the minerals and their corresponding hydrothermal alteration type is based on this spectral property.

Pre-processing of satellite images was performed on ASTER, Sentinel-2A and IKONOS dataset. These images were already georeferenced with an acceptable accuracy. According to Mars and Rowan (2006), the band 5 of ASTER shows somewhat lower than actual value. Therefore, the average amount of 7.9% was added to this band according to Shahriari et al. (2013). After correction of the band 5 of ASTER, these images were corrected geometrically. Further, atmospheric corrections were applied to all images. To process the images of Sentinel-2A, IKONOS and 5-bands of TIR in ASTER, Internal Average Relative Reflectance (IARR) correction and on the SWIR bands and VNIR bands of ASTER, the Fast Line-of-sight Atmospheric Analysis of Spectral Hypercubes (FLAASH) atmospheric correction were performed respectively

.

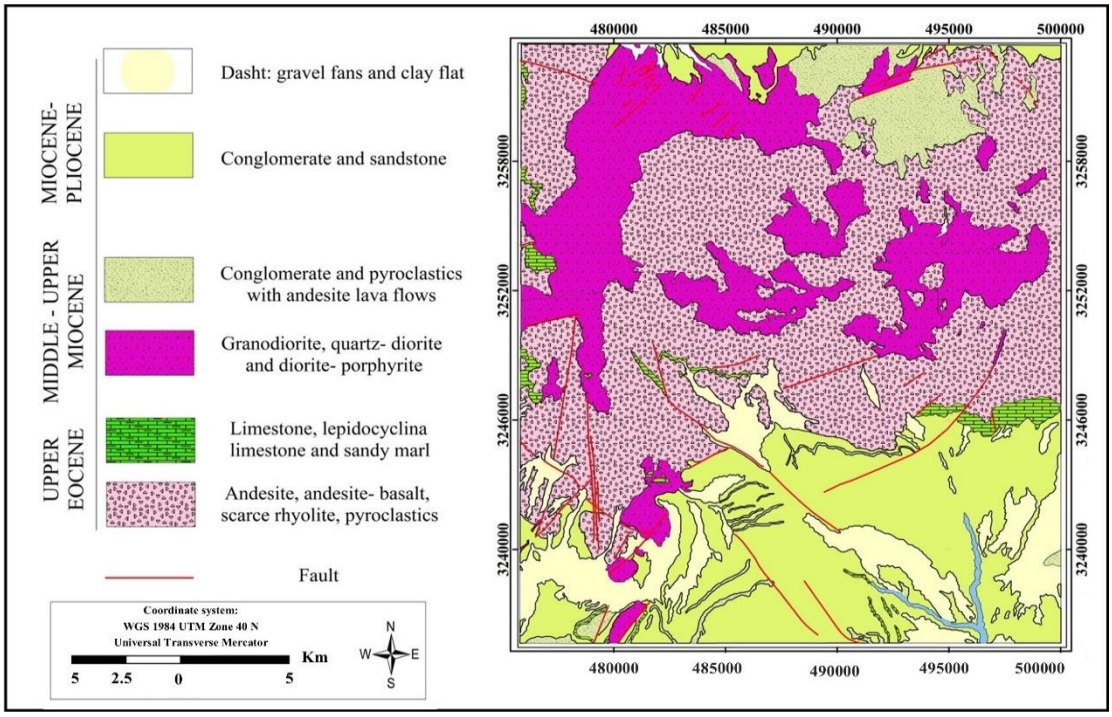

Figure 1. Rabor Geology Map (adapted from Sridic, et al.1972).

Spectral Feature Fitting (SFF) method was used to identify the minerals in the zones of hydrothermal alterations (Clark and Roush, 1984). SFF is a method that has a great application in the mapping of minerals and an efficient way of comparing absorption features in the image spectrum and the reference spectrum (library or sample derived spectra) (Clark and Roush, 1984; Abbaszadeh and Hezarkhani, 2013; Zamyad et al., 2019). This method is used in this research to enhance hydrothermal alteration minerals by using ASTER ASTER images. The similarity and conformity between the image spectrum and the reference spectrum is studied by investigating samples' spectra of the known signature and the recorded spectrum for each pixel in the ASTER image (Zamyad et al., 2019).

PCA is a statistical tool that uses multispectral bands for reducing the data size and for mapping different hydrothermal alteration types. This method calculates the eigenvectors of a covariance or a correlation matrix. PCA has been extensively applied for hydrothermal alteration mapping in metallogenic provinces (e.g., Bhadra et al., 2013; Tangestani and Moore, 2001; Crosta et al. 2003: Yousefi et al., 2018a) in such a way that it is applied to multivariate data such as multispectral satellite images to discriminate the spectral responses associated with specific hydrothermal alteration minerals. In order to reduce the amount of data and extract more information from the targets with certain properties such as the hydrothermal areas that contained iron oxides also, selected bands of Sentinel-2A and ASTER data were used. These bands were stacked and then used in the PCA.

GMPI is used as a potential mapping method. The basis of this method is the stepwise PC selection by the principal component Analysis. Therefore, the step-wise factor analysis was applied to the stream geochemical data and determined factors that represented Cu concentration in the stream sediments. The map of factors correlated with Cu converted to fuzzy according to equation (1) and GMPI was achieved.

$$GMPI_{F_n} = \frac{e^{FS_n}}{1+e^{FS_n}} \quad (1)$$

Here, Fn is equal to the factor n-m and FSn is equal to the factor n-m scores (Yousefi et al., 2012)

4. Results

4.1. Spectral Feature Fitting

To use the SFF method, the corrected ASTER images were used. To do this, we first sampled 37 points from the study area. By studying the thin sections prepared from each of the samples, 16 samples were selected for spectroscopy using the FieldSpec® 3 spectrophotometer. Selection of these 16 samples was based on the presence of at least one of the hydrothermal alteration types mentioned above and also iron oxides minerals. The spectra measured on the samples were used here as the reference spectra. The mineral spectra of each of the sericitic, argillic, and propylitic hydrothermal alterations and gossans are presented in Figure 2.

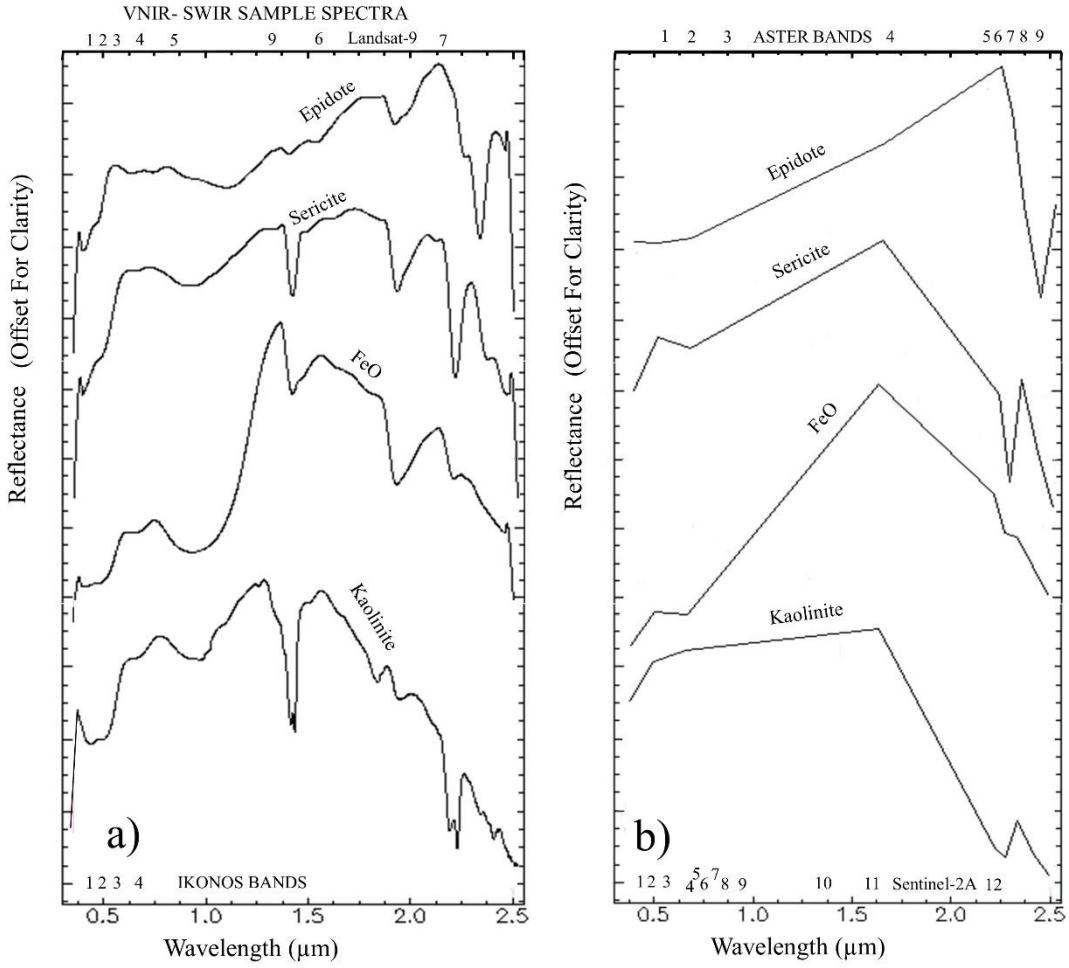

Figure 2. Spectra of minerals (based on ASTER bands) related to areas of sericitic, argillic, and propylitic alterations and iron oxide minerals. a) measured on samples and b) resampled spectra based on ASTER bands.

The map derived from the application of these spectra are shown in Figure 3. In this figure, Sericite as one of the major hydrothermal minerals, is representing sericitic alteration in figure 3a, Kaolinite representing argillic alteration in figure 3b and epidote indicating a propylitic alteration in figure 3c.

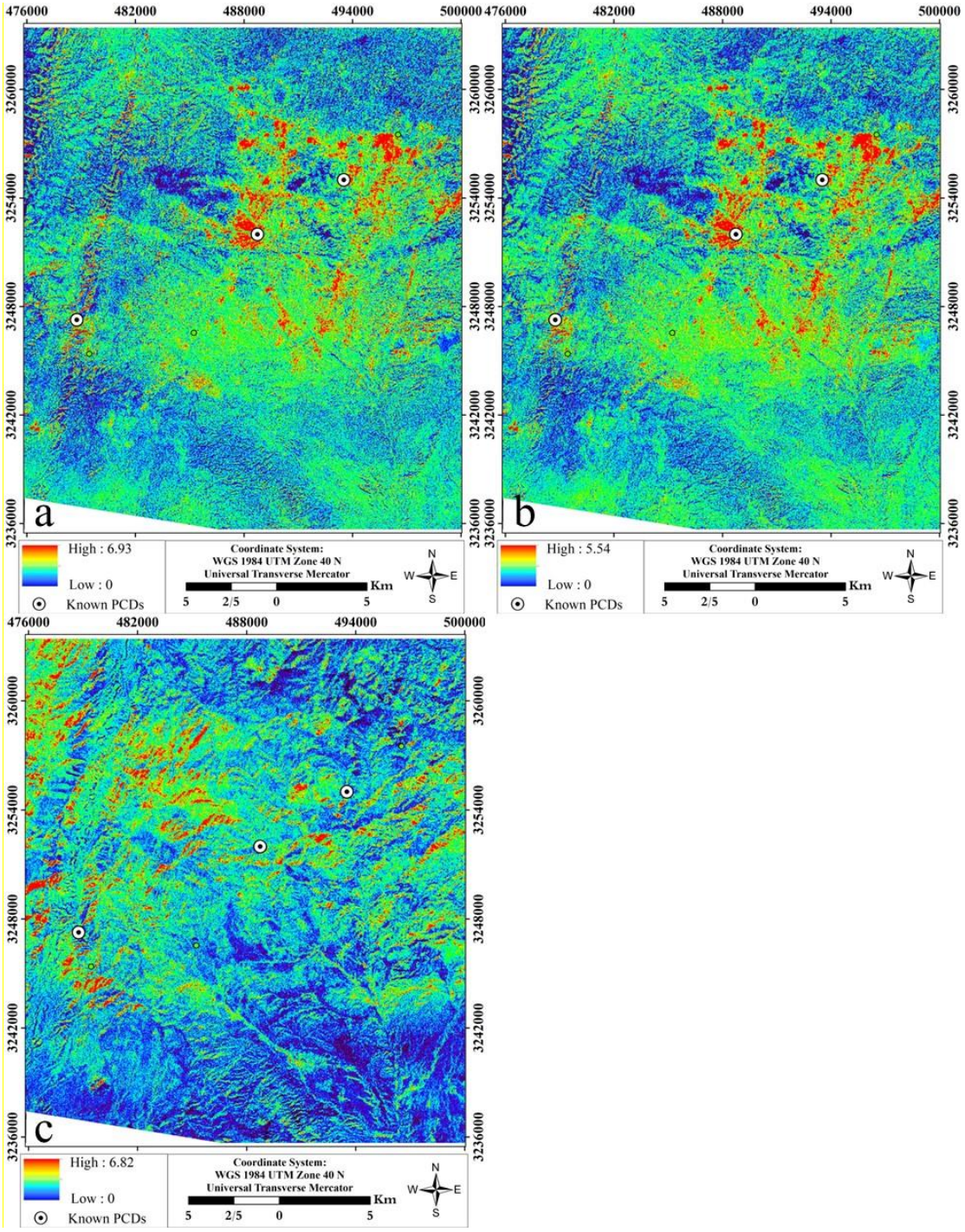

Figure 3. The results of SFF for hydrothermal alterations a) serisitic alteration, b) argillic alteration and c) propylitic alteration. PCD = Porphyry Copper Deposit.

4.2. Iron oxides enhancement

To illustrate the iron oxides, we can use the three images of ASTER, Sentinel-2A and IKONOS, with spatial resolution of 15, 10 and 1 meters respectively. The highest intensity of reflection of iron oxides in the red band (0.665 micrometer) and the minimum reflection (absorption) at 0.443 micrometers in the blue range. Due to the absence of a wavelength (blue range), ASTER images can't show iron oxides as good as other satellite images that have this band. As a result, in this study, the b4 / b2 ratio, which indicates the maximum reflection to the lowest reflection, was used to enhance the iron oxides minerals using Sentinel-2A. In Figure 4, the enhanced iron oxides with the help of Sentinel-2A images are shown in red colour.

Iron oxides can also be seen with the help of the IKONOS image. Figure 5 shows the iron oxide present in the Abdar area (center of the region). This image has been extracted using b3/b1 ratio.

4.3. Combined Selective Principal Component Analysis

Separation of iron oxide impregnated outcrops was done by the combination of selective bands of Sentinel-2A and ASTER bands as well as the combination of Landsat 9 and ASTER bands. Therefore, selective PCA was used. The results of the combination of ASTER and Sentinel-2A bands following the application of selective PCA show that the iron oxide impregnated outcrops are enhanced better than the results obtained by the combination of ASTER and Landsat 9 bands.

Therefore, only the results from the combination of ASTER and Sentinel-2A bands are described here. The second and the fourth Sentinel-2A bands with wavelengths of 0.490 and 0.665 μm, respectively, were combined with the ASTER bands associated with argillic and phyllic hydrothermal alteration types. The result of PCA for these selected bands of ASTER and Sentinel-2A data are presented in Table 1

.

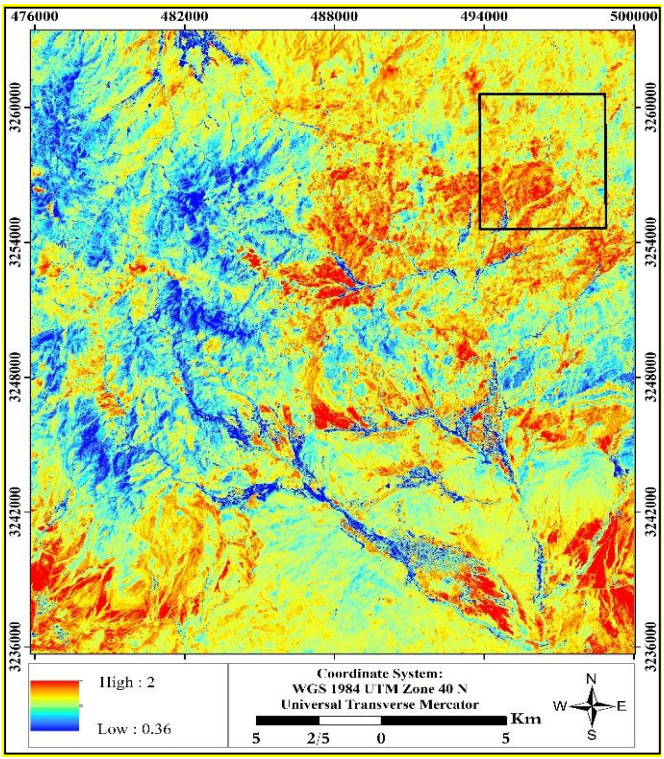

Figure 4. Iron oxide (red), using b4 / b2 ratio from Sentinel-2A satellite images. The rectangle shows the area covered in Figure 5.

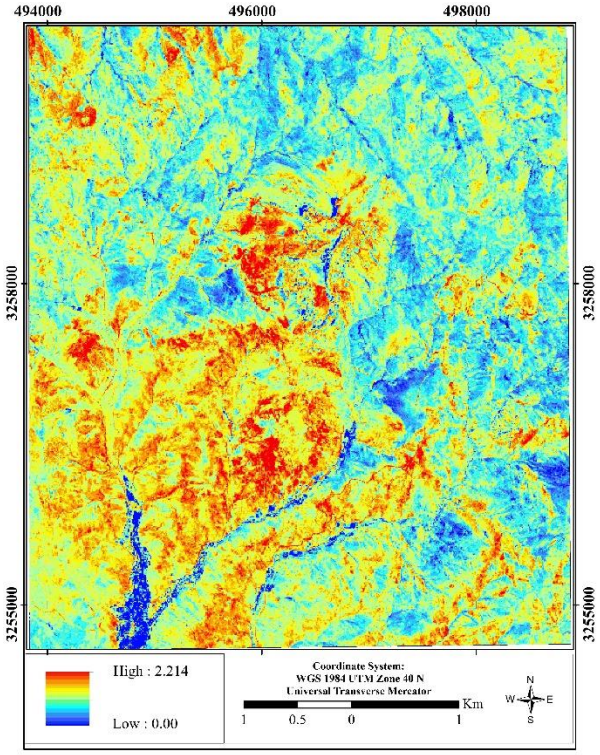

Figure 5. The iron oxides (red), using b3 / b1 ratio on IKONOS satellite images.

Table 1. The results of the combination of selected bands of Sentinel-2A and ASTER bands using Selective PCA for the enhancements of the hydrothermally altered outcrops coated with iron oxide minerals.

(a)- Argillic					(b)- Phyllic (sericitic)				
	EIGENVECTOR					EIGENVECTOR			
	PC1	PC2	PC3	PC4		PC1	PC2	PC3	PC4
Band $2_{\text{Sentinel- 2A}}$	-0.08	0.58	0.22	0.78	Band $2_{\text{Sentinel- 2A}}$	0.10	-0.57	-0.39	-0.71
Band $4_{\text{Sentinel- 2A}}$	-0.13	0.80	-0.20	-0.55	Band $4_{\text{Sentinel- 2A}}$	0.16	-0.80	0.27	0.51
Band 4_{ASTER}	-0.77	-0.14	-0.60	0.19	Band 6_{ASTER}	0.70	0.13	-0.62	0.33
Band 5_{ASTER}	-0.62	-0.07	0.75	-0.22	Band 7_{ASTER}	0.69	0.13	0.62	-0.34
Eigenvalue	75.87	22.08	1.34	0.71	Eigenvalue	76.10	23.19	0.90	0.81
Variance (%)	3	6	16	11	Variance (%)	3	6	13	12

Equations 1 and 2 represent each of the hydrothermal alterations along with the iron oxides.

(1) $-PC3 = -0.22B2_{S-2A} + 0.20B4_{S-2A} + 0.60B4_{ASTER} - 0/75B5_{ASTER} \Rightarrow$ Argillic alteration + FeO

(2) $PC3 = -0.39B2_{S-2A} + 0/27B4_{S-2A} - 0.62B6_{ASTER} + 0.62B7_{ASTER} \Rightarrow$ Phyllic alteration + FeO

Figure 6 is prepared based on the equations 1 and 2 that shows areas with advanced argillic (red) and intense sericitic (green) alteration types that are coated with iron oxide minerals.

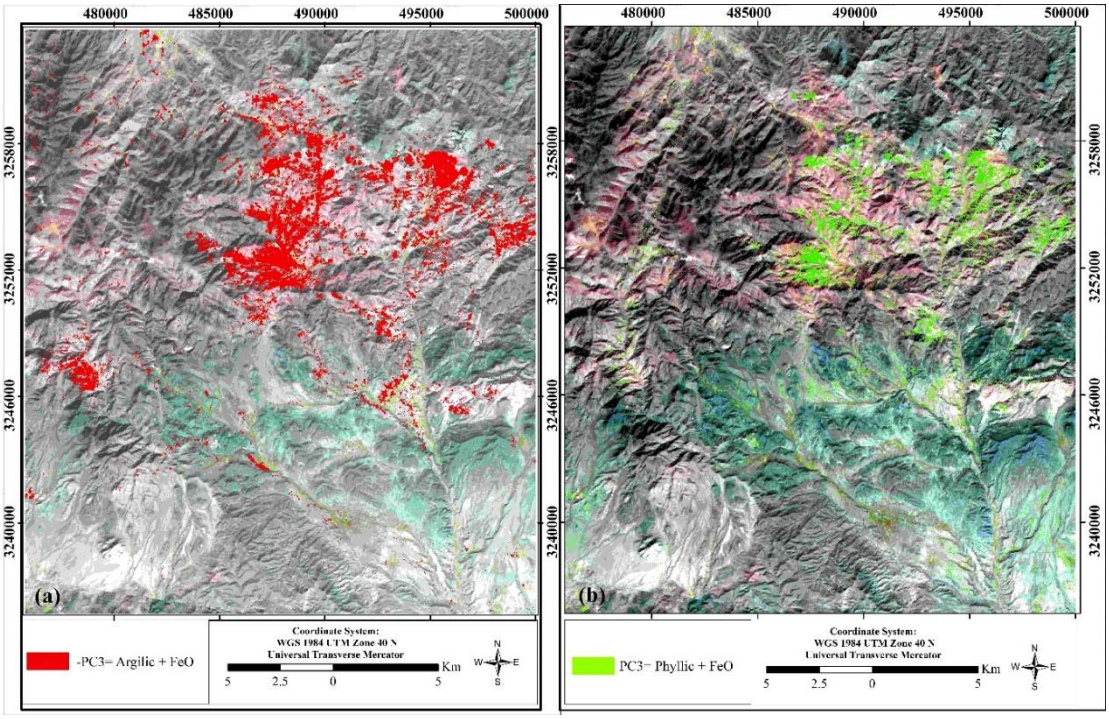

Figure 6. Map of hydrothermally altered areas that are coated with iron oxide minerals. These maps are prepared based on equations 1 and 2.

4.4. GMPI (Geochemical Mineral Potential Index)

Initially, PCA analysis was applied on 49 chemical elements from Rabor geological sheet and eight PCs were selected based on Eigenvalues less than 1. Considering the high values of Cu and Au in factor two, this factor was considered as an indicator factor for the presence of these elements and as a basic factor. Elements of this factor and other factors correlated with this factor (including factors 4 and 5) were kept. Therefore, other elements have been removed from the process. The high correlation between elements of factor one, due to the lithological effect, was not considered in subsequent processing. After performing the factor analysis using the PCA method and selecting the elements correlated with Cu, 25 elements remained for further processing and other elements were removed. By repeating the previous method on 25 elements, five PCs were selected. In Table 2, The factors derived from the second stage factor analysis along with the correlated elements with factors are shown. Then, the maps of PCs 4 and 2 were drawn. Since the maps of PCs 4 and 2 are in numerical intervals [-0.2, 4] and [-11, 6]; The GMPI index was converted into fuzzy values. Then the GMPI map was drawn according to PCs 4 and 2. The final GMPI_4 and GMPI_2 maps are shown in Figure 7.

GMPI_4 shows Cu, Au, Re, Bi, IN and Te mineralization and GMPI_2 shows Ag, Cd, Cu, Hg, IN, Mn, Pb, Zn and Sb mineralization. The areas with red and yellow colors represent the regions with abnormal Cu and Cu-related elements. In Figure 7, the GMPI index separates the mineralization areas of Chehren, North Chehren, Qanat marvan, Saghadin and Tidar from other regions. This shows that the GMPI index can be used as a technique for mineral exploration.

Table 2. Results of stage-wise PCA.

Rotated Component Matrix					
	Component				
	1	2	3	4	5
Au	0.21	0.255	0.237	0.545	-0.325
Ag	0.345	0.729	0.391	0.183	0.063
As	0.221	0.166	0.635	0.314	-0.051
Bi	0.734	0.177	0.047	0.454	-0.148
Ca	-0.666	-0.089	-0.222	-0.308	0.268
Cd	0.534	0.635	0.346	0.027	-0.28
Cs	0.124	0.093	0.903	0.068	-0.08
Cu	0.121	0.376	0.297	0.691	-0.132
Hf	-0.425	-0.129	-0.087	-0.275	0.765
Hg	-0.133	0.467	0.357	0.075	0.484
IN	0.151	0.6	-0.054	0.496	-0.071
Li	-0.207	-0.007	0.851	-0.087	0.036
Mn	-0.399	0.703	0.038	0.027	-0.329
Mo	0.843	0.119	-0.138	0.295	-0.141
Pb	0.481	0.74	0.264	0.085	-0.119
Re	0.461	-0.128	-0.066	0.717	-0.063
S	0.623	0.135	0.205	0.316	-0.038
Sb	0.391	0.458	0.61	0.211	-0.043
Se	0.658	0.033	-0.028	0.224	-0.234
Sr	-0.359	-0.245	-0.35	-0.229	0.335
Te	0.552	0.272	0.19	0.44	-0.124
TL	0.823	0.144	0.374	0.103	-0.163
W	0.806	-0.085	-0.092	-0.253	-0.271
Zn	0.2	0.926	-0.024	0.102	0.084
Zr	-0.502	-0.075	-0.105	-0.178	0.761
Eigenvalue	10.25	3.65	2.05	1.25	1.20
Variance (%)	24.294	16.549	13.505	10.856	8.609

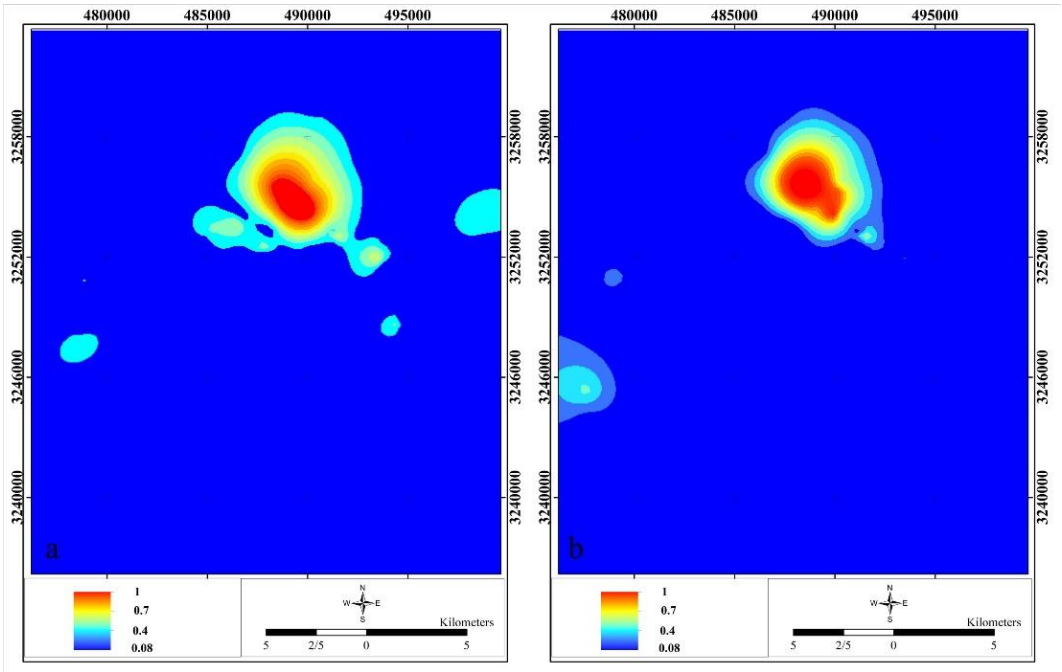

Figure 7. Maps of GMPI index; (a) GMPI_4 shows Cu, Au, Re, Bi, IN and Te mineralization and (b) GMPI_2 shows Ag, Cd, Cu, Hg, IN, Mn, Pb, Zn and Sb mineralization.

5. Field observations and validation

To validate the results obtained by remote sensing and geochemical data, hydrothermal alteration types enhanced by remote sensing techniques were observed in the field and 37 rock samples were collected for further laboratory studies. Thin sections were prepared from these samples and then, spectra of 16 samples measured using FieldSpec® 3 spectroradiometer. Figures 8a and 8b show the photograph of outcrops with hydrothermal alteration in the Saghadin area. Figure 8c shows the photograph of a thin section obtained from the RAB-25 sample; in which the quartz, sericite and iron oxide (in the form of transverse vein) minerals are clearly identified. The existence of a transverse vein can indicate the presence of Cu mineralization in the area. In Figure 8d, the spectrum of the sample RAB-25 is shown, that is belong to a sample with sericite and iron oxide minerals. Figures 9a also shows the photograph of outcrops with sericitic and argillic alteration in the Chehren area. Figure 9b shows the photograph of a thin section obtained from the RAB-13 sample; that shows clouding due to presence of kaolinite. In Figure 9c, the spectrum obtained from the RAB-13 sample, which shows typical double absorption for kaolinite.

Based on the remote sensing and geochemical data, the altered and mineralized regions in the Rabor area can be divided into eight areas that can be used for further mineral exploration, including QanatMarvan, Chehren, North Chehren, Abdar, Pay Negin, Saghadin, Tidar and Izad Abad (Figure 10).

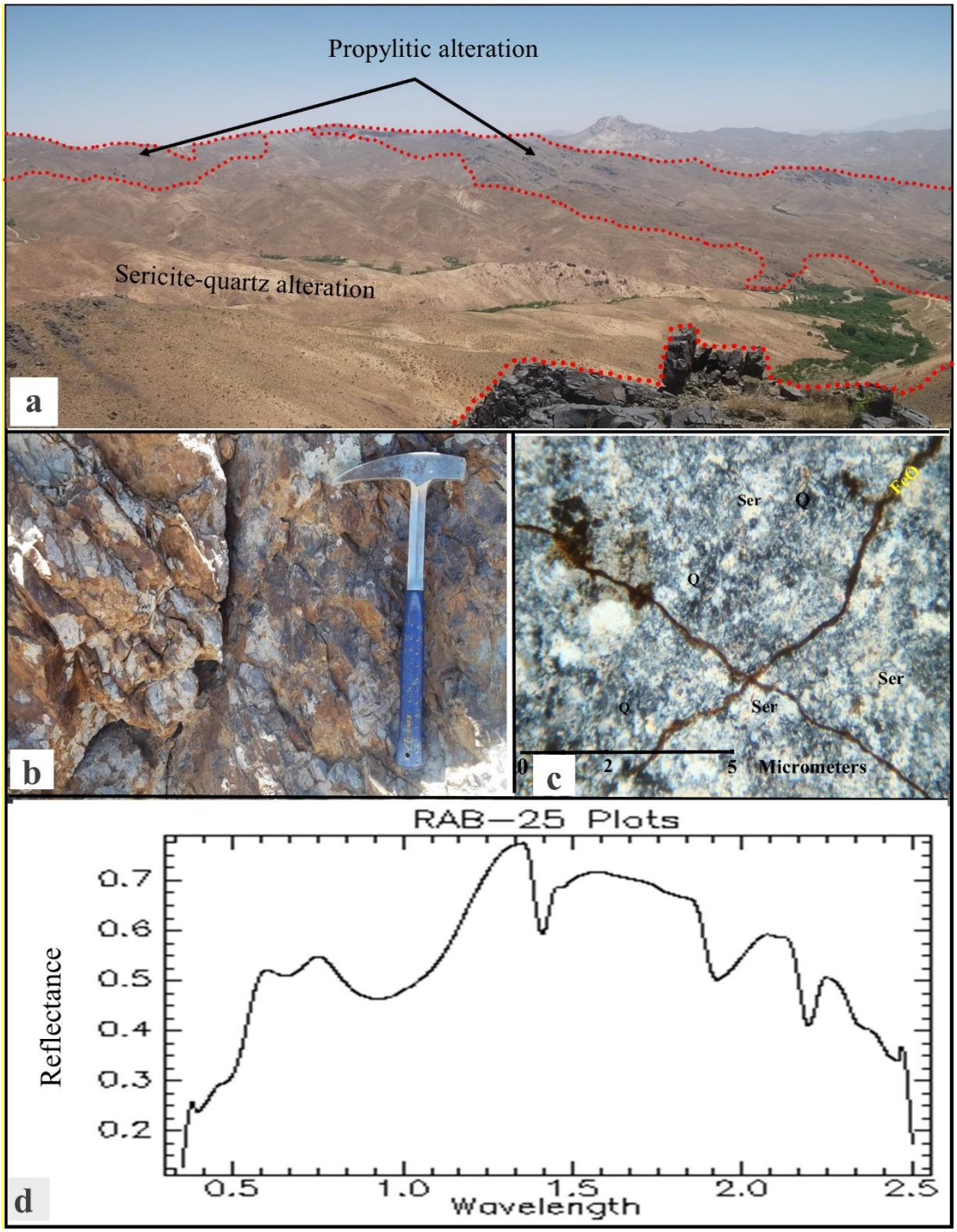

Figure 8. (a)Panoramic view of the outcrops with hydrothermal alteration in Saghadin area (viewing north east); (b) an outcrop with sericite-quartz alteration coated with iron oxide minerals; (c) Thin section obtained from RAB-25 specimen, and (d) Spectrum obtained from the RAB-25 specimen.

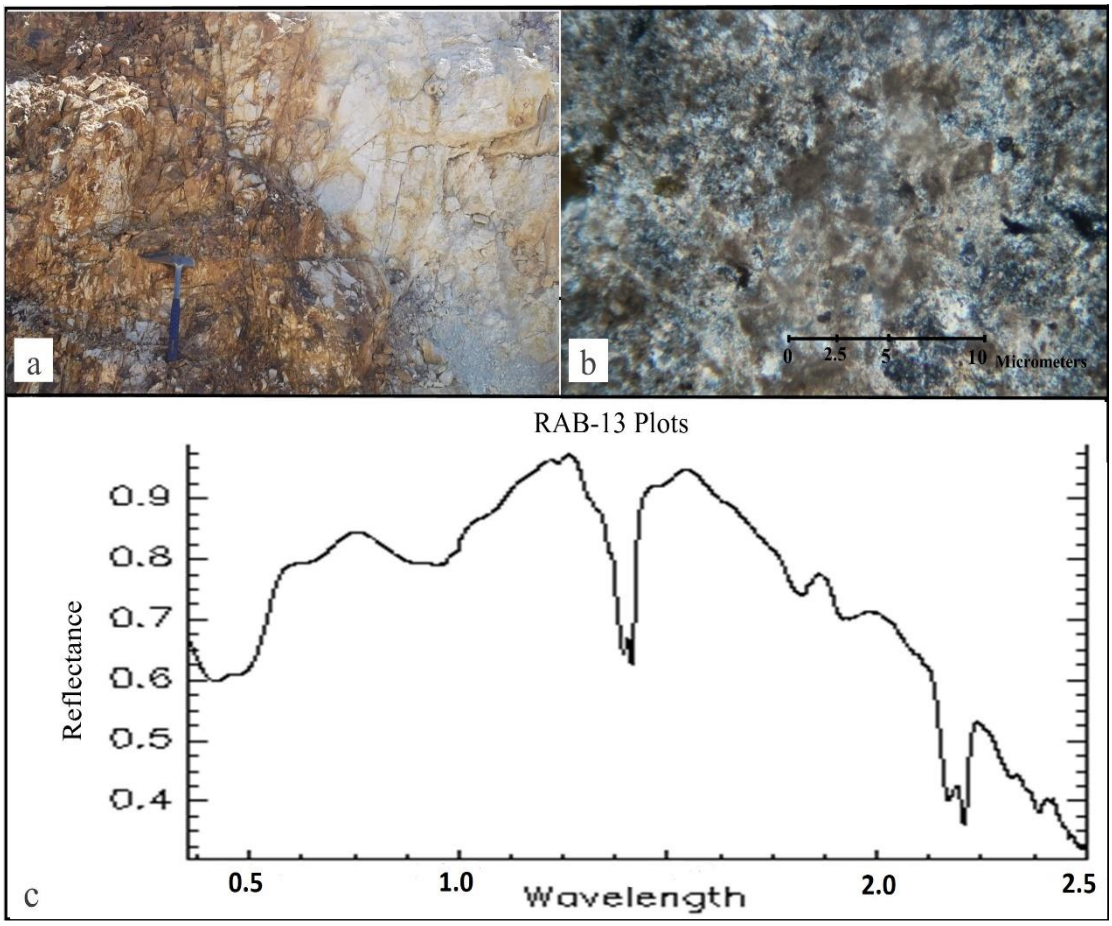

Figure 9. (a) Photograph of an outcrop in Chehren area; (b) thin section obtained from RAB-13 that shows clouding due to presence of kaolinite and (c) spectrum obtained from the RAB-13 specimen that show typical double absorption for kaolinite.

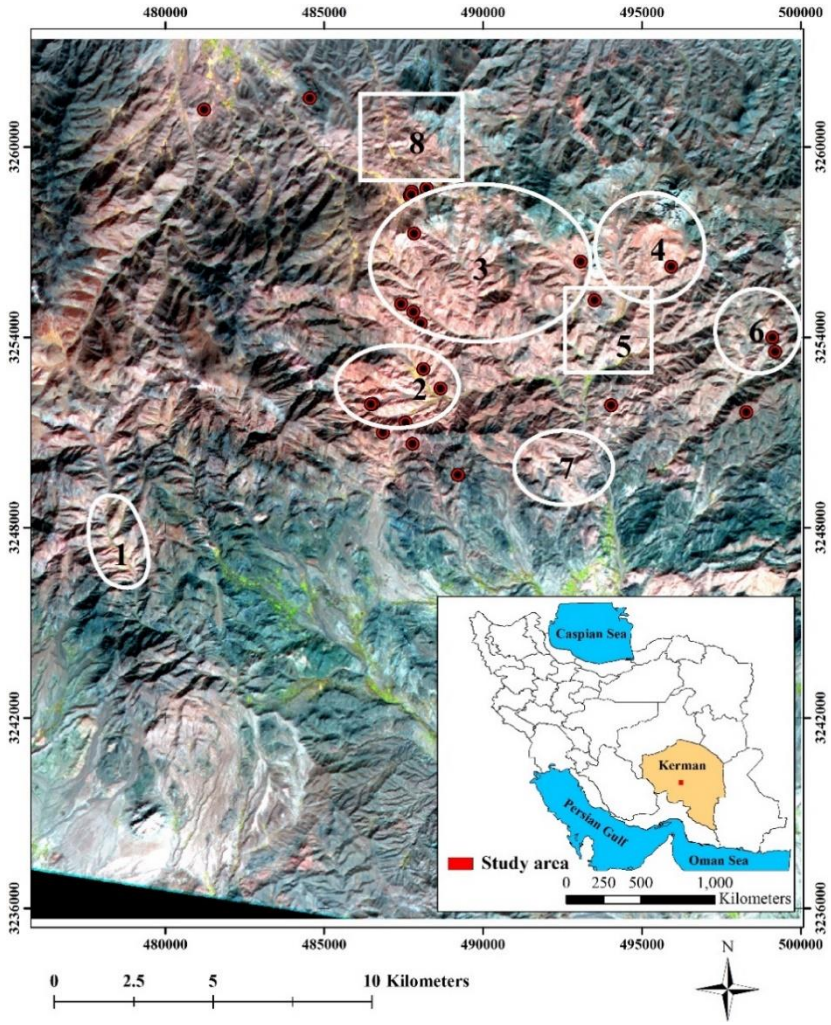

Figure 10. Location of alterations and mineralization areas in the study area, location of the samples is indicated in the picture by brown circles (1. QanatMarvan, 2. Chehren, 3. North Chehren, 4. Abdar, 5. Pay Negin, 6. Saghadin, 7. Tidar, 8. Izad Abad). The areas are shown on the ASTER images, R, G, B = 4, 6, 8.

6. Discussion

To demonstrate hydrothermal alterations, SFF method was used based on spectra from the samples, using ASTER images and argillic, sericite, and propylitic alterations were identified. Based on the field observations and laboratory studies, kaolinite and montmorillonite were observed in the argillic alteration zone.

Quartz and sericite minerals are indicators of sericitic alteration. Epidote, chlorite and calcite minerals are also indicators of propylitic alteration and this type of alteration is more in the margins of the argillic and phyllic zones. Siliceous alteration also has a wide overlap with argillic and sericitic alterations. Sericitic alteration index minerals such as quartz and sericite are closely related to mineralization regions.

Based on these results, there were a lot of overlapping between sericitic and argillic alterations in the region. The existence of this overlap was due to the secondary weathering of rocks and minerals with sericite alteration that transformed to clay minerals such as Kaolinite and Montmorillonite. Among the methods used, the SFF method was better for separating the hydrothermal alteration zones. The CSPCA method

was also good for hydrothermal alteration. This was due to the greater association of these areas with advanced argillic and intense sericitic alterations. In the northern regions of the Rabor area, alterations had not been evident using any of the processing methods; because the dense vegetation cover of this area.

Along with each of these alterations, iron oxides were well observed in the processed satellite images. The spatial resolution of each image with bands of 0.665 and 0.443 micrometers plays a decisive role in better enhancement of iron oxides. Due to the fact that IKONOS has spectral bands in 0.680 and 0.490 micrometers and its spatial resolution is 1 meter, Therefore, first with the help of the images of IKONOS and then the images of Sentinel-2A, iron oxides were enhanced. The areas with both hydrothermal alteration and iron oxide minerals coating were well correlated with the known mineralized areas.

By comparing the geochemical data (GMPI maps) and remote sensing results, it was found that these two were reasonably correlated. Although the stream geochemical data is dynamic and dislocated. Each of these data can be used to explore areas with vein and porphyry type copper mineralization. However, the processed remote sensing data had higher correlation with the known mineralization than the GMPI index map applied to the stream geochemical data. After examining the remote sensing and geochemical data, few areas were suggested for further detailed mineral exploration.

7. Summary and conclusions

There are several results have been found out by conducting this research as shown in the following:

1. IKONOS was best for iron oxide mapping due to its spectral and spatial resolutions.
2. Among the methods used, the SFF method was better for separating the hydrothermal alteration zones. In order to identify hydrothermally altered outcrops coated with iron oxide minerals, which are directly related to porphyry copper areas, CSPCA method was quite useful.
3. The field data shows that due to the vegetation cover in parts of the area, all areas with hydrothermal alteration can't be properly identified through the processing of satellite imageries.
4. The GMPI index applied to the stream geochemical data can be used as an index for mineral potential mapping.
5. Comparing the results obtained from various data, the results of remote sensing data show better than geochemical data to determine areas with porphyry copper mineralization.
6. Based on the analysis of remote sensing and geochemical data, few areas were suggested for further detailed exploration, among which, the Saghadin area is more promising.

8.References

Abbaszadeh M, Hezarkhani A. Enhancement of hydrothermal alteration zones using the spectral feature fitting method in Rabor area, Kerman, Iran. Arabian Journal of Geosciences. 2013; 6:1957-64.

Abrams MJ, Brown D, Lepley L, Sadowski R. Remote sensing for porphyry copper deposits in southern Arizona. Economic Geology. 1983; 78(4): 591-604.

Alimohammadi M, Alirezaei S, Kontak DJ. Application of ASTER data for exploration of porphyry copper deposits: A case study of Daraloo–Sarmeshk area, southern part of the Kerman copper belt, Iran. Ore Geology Reviews. 2015; 70: 290-304.

Atapour H, Aftabi A. The geochemistry of gossans associated with Sarcheshmeh porphyry copper deposit, Rafsanjan, Kerman, Iran: implications for exploration and the environment. Journal of Geochemical exploration. 2007; 93(1): 47-65.

Bhadra BK, Pathak S, Karunakar G, Sharma JR. ASTER data analysis for mineral potential mapping around Sawar-Malpura area, Central

Rajasthan. Journal of the Indian Society of Remote Sensing. 2013; 41(2): 391-404.

Bahrami Y, Hassani H, Maghsoudi A. Investigating the capabilities of multispectral remote sensors data to map alteration zones in the Abhar area, NW Iran. Geosystem Engineering. 2021; 24(1): 18-30.

Chen Q, Xia J, Zhao Z, Zhou J, Zhu R, Zhang R, Zhao X, Chao J, Zhang X, Zhang G. Interpretation of hydrothermal alteration and structural framework of the Huize Pb–Zn deposit, SW China, using Sentinel-2, ASTER, and Gaofen-5 satellite data: implications for Pb–Zn exploration. Ore Geology Reviews. 2022: 150(105154).

Clark RN, Roush TL. Reflectance spectroscopy: Quantitative analysis techniques for remote sensing applications. Journal of Geophysical Research: Solid Earth. 1984; 89(B7): 6329-40.

Crosta AP, De Souza Filho CR, Azevedo F, Brodie C. Targeting key alteration minerals in epithermal deposits in Patagonia, Argentina, using ASTER imagery and principal component analysis. International journal of Remote sensing. 2003; 24(21): 4233-40.

Dimitrijevic MD. Geology of Kerman region: institute for geological and mining exploration and investigation of nuclear and other mineral raw material, Beograd—Yugoslavia, Iran Geol. Survey Rept Yu/52. 1973.

Gupta RP. Multispectral Imaging Systems. In Remote Sensing Geology. Springer. Berlin, Heidelberg; 2003. P 75-122.

Honarmand M, Ranjbar H, Shahabpour J. Combined use of ASTER and ALI data for hydrothermal alteration mapping in the northwestern part of the Kerman magmatic arc, Iran. International Journal of Remote Sensing. 2013; 34(6): 2023-46.

Honarmand M, Ranjbar H, Shahriari H, Naseri F. Evaluating the effect of using different reference spectra on SAM classification results: an implication for hydrothermal alteration mapping. Journal of Mining and Environment. 2018; 9(4): 981-97.

Jain N, Singh R, Roy P, Martha TR, Vinod Kumar K, Chauhan P. Mapping of hydrothermally altered zones in Aravalli Supergroup of rocks around Dungarpur and Udaipur, India, using Landsat-8 OLI and spectroscopy. Arabian Journal of Geosciences. 2018; 11(16): 1-4.

Khaleghi M, Ranjbar H, Abedini A, Calagari AA. Synergetic use of the Sentinel-2, ASTER, and Landsat-8 data for hydrothermal alteration and iron oxide minerals mapping in a mine scale. Acta Geodyn. Geromater. 2020; 17: 311-29.

Lowell JD, Guilbert JM. Lateral and vertical alteration-mineralization zoning in porphyry ore deposits: Economic Geology; 1970; 65(4): 373-408.

Mars JC, Rowan LC. Regional mapping of phyllic- and argillic-altered rocks in the Zagros magmatic arc, Iran, using Advanced Spaceborne Thermal Emission and Reflection Radiometer (ASTER) data and logical operator algorithms. Geosphere. 2006; 2(3): 161-86.

Masoumi F, Eslamkish T, Honarmand M, Abkar AA. A comparative study of landsat-7 and landsat-8 data using image processing methods for hydrothermal alteration mapping. Resource Geology. 2017; 67(1): 72-88.

Shahriari H, Ranjbar H, Honarmand M. Image segmentation for hydrothermal alteration mapping using PCA and concentration–area fractal model. Natural Resources Research. 2013; 22(3): 191-206.

Sridic A, Dimitrijevic MN, Cvetic S, Dimitrijevic MD. Geological map of baft (1: 100,000). Geological Survey of Iran. 1972.

Tangestani MH, Mazhari N, Agar B. Mapping the porphyry copper alteration zones at the Meiduk area, SE Iran, using the advanced spaceborne thermal emission and reflection radiometer (ASTER) data. In Remote Sensing for Environmental Monitoring, GIS Applications, and Geology. 2005; 5983: 172-181.

Tangestani MH, Moore F. Comparison of three principal component analysis techniques to porphyry copper alteration mapping: a case study, Meiduk area, Kerman, Iran. Canadian journal of remote sensing. 2001; 27(2):176-82.

Van der Werff H, Van der Meer F. Sentinel-2A MSI and Landsat 8 OLI provide data continuity for geological remote sensing. Remote sensing. 2016; 8(11): 883.

Vuolo F, Żółtak M, Pipitone C, Zappa L, Wenng H, Immitzer M, Weiss M, Baret F, Atzberger C. Data service platform for Sentinel-2 surface reflectance and value-added products: System use and examples. Remote Sensing. 2016; 8(11): 938.

Yan L, Roy DP, Zhang H, Li J, Huang H. An automated approach for sub-pixel registration of Landsat-8 Operational Land Imager (OLI) and Sentinel-2 Multi Spectral Instrument (MSI) imagery. Remote Sensing. 2016; 8(6): 520.

Yousefi M, Kamkar-Rouhani A, Carranza EJ. Geochemical mineralization probability index (GMPI): a new approach to generate enhanced stream sediment geochemical evidential map for increasing probability of success in mineral potential mapping. Journal of Geochemical Exploration. 2012; 115: 24-35.

Yousefi SJ, Ranjbar H, Alirezaei S, Dargahi S, Lentz DR. Comparison of hydrothermal alteration patterns associated with porphyry Cu deposits hosted by granitoids and intermediate-mafic volcanic rocks, Kerman Magmatic Arc, Iran: Application of geological, mineralogical and remote sensing data. Journal of African Earth Sciences. 2018a; 142: 112-23.

Yousefi T, Aliyari F, Abedini A, Calagari AA. Integrating geologic and Landsat-8 and ASTER remote sensing data for gold exploration: a case study from Zarshuran Carlin-type gold deposit, NW Iran. Arabian Journal of Geosciences. 2018b; 11(17): 1-9.

Zamyad M, Afzal P, Pourkermani M, Nouri R, Jafari MR. Determination of hydrothermal alteration zones using remote sensing methods in Tirka Area, Toroud, NE Iran. Journal of the Indian Society of Remote Sensing. 2019; 47: 1817-30.